

The Prism Hypothesis: Harmonizing Semantic and Pixel Representations via Unified Autoencoding

Weichen Fan^{1,2} Haiwen Diao¹ Quan Wang² Dahua Lin² Ziwei Liu^{1,✉}

¹S-Lab, Nanyang Technological University ²SenseTime Research

weichen002@e.ntu.edu.sg, haiwen.diao@ntu.edu.sg,

{wangquan, dhlin}@sensetime.com, ziwei.liu@ntu.edu.sg



Github: <https://github.com/WeichenFan/UAE>.

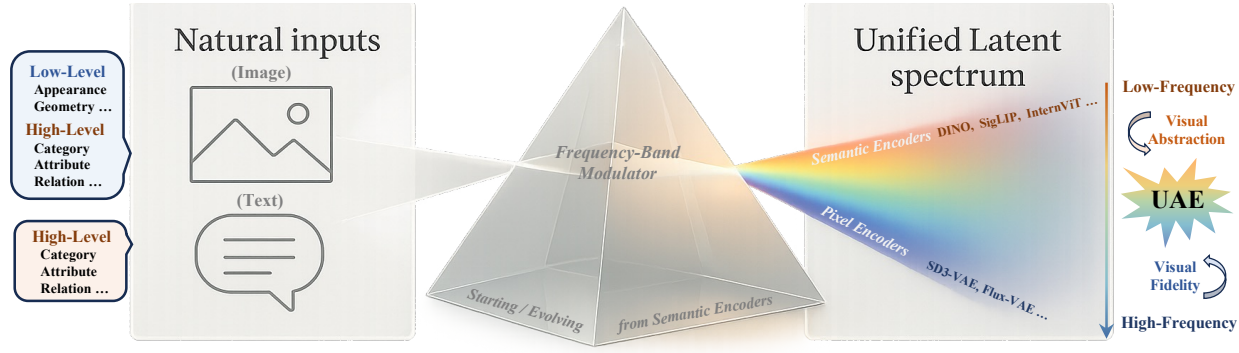


Figure 1. The Prism Hypothesis. Our conceptual “prism” decomposes various natural inputs into spectral components along frequency. Low frequency bands capture global semantics and abstract meaning, while high frequency bands encode local detail and fine visual texture. This motivates our Unified Autoencoding (UAE), which harmonizes semantic and pixel representations within a single latent space.

Abstract

Deep representations across modalities are inherently intertwined. In this paper, we systematically analyze the spectral characteristics of various semantic and pixel encoders. Interestingly, our study uncovers a highly inspiring and rarely explored correspondence between an encoder’s feature spectrum and its functional role: semantic encoders primarily capture low-frequency components that encode abstract meaning, whereas pixel encoders additionally retain high-frequency information that conveys fine-grained detail. This heuristic finding offers a unifying perspective that ties encoder behavior to its underlying spectral structure. We define it as **the Prism Hypothesis**, where each data modality can be viewed as a projection of the natural world onto a shared feature spectrum, just like the prism. Building on this insight, we propose **Unified Autoencoding (UAE)**, a model that harmonizes semantic structure and pixel details via an innovative frequency-band modulator, enabling their seamless coexistence. Extensive experiments on ImageNet and MSCOCO benchmarks validate that our UAE ef-

fectively unifies semantic abstraction and pixel-level fidelity into a single latent space with state-of-the-art performance.

1. Introduction

Trained on massive corpora, recent foundation models have profoundly reshaped perception and generation systems, generalizing well across diverse downstream tasks [3, 25, 26, 29]. Yet, early advances in perception and generation evolve along largely separate trajectories. Their objectives are typically distributed across distinct network structures, e.g., employing pretrained semantic encoders [3, 26, 29], to capture high-level meaning, or pixel encoders [19, 31] to compress fine-grained visual detail. While each module excels within its own domain, this fragmentation compels subsequent unification efforts [11, 28, 39] to depend simultaneously on semantic and pixel encoders, forcing networks to reconcile fundamentally heterogeneous representations. The sharp mismatch lowers training efficiency and induces representational conflicts, with these incompatible features often interfering rather than complementing one another.

This fragmentation uncovers a deep-seated tension between abstraction and fidelity, which is a driving force in shaping subsequent foundation models. To alleviate it, recent studies [34, 48, 50] attempt to transfer semantic encoders into visual generation domains alongside strong pixel decoders. This strategy substantially accelerates convergence and improves semantic correspondence, yet remains limited in recovering fine-grained visual details. In parallel, another research direction seeks to endow pixel encoders with semantic awareness through text supervision [43, 44, 46], semantic encoder distillation [4, 12], and hierarchical feature integration [43]. While these efforts move toward unifying understanding and generation representations in a single module, they often achieve coexistence through trade-offs rather than genuine integration.

At the core of this development lies a fundamental question: How is information about the world represented such that multimodal inputs share a common semantic meaning while preserving their native granularity of detail?

Impressively, we empirically observe that pre-trained semantic features, whether derived from text or vision, tend to reside at the coarse end of the decoupled feature spectrum, primarily capturing low-frequency structures such as categories, attributes, and relations. In contrast, pre-trained pixel-level features extend toward the finer end of the spectrum, representing higher-frequency components that convey intricate appearance and geometric detail. Strikingly, these complementary representations can be harmoniously integrated within a unified encoder, extremely aligning well with the spectral arrangement and fostering a progressive synergy from semantic perception to detailed reconstruction. We posit this as *the Prism Hypothesis* in Figure 1: the real-world inputs project onto a continuous shared feature spectrum, and what we perceive as different modalities are distinct slices of this underlying continuum.

From this perspective, we introduce **Unified Autoencoding (UAE)**, a tokenizer that learns a shared latent space and harmonizes semantic structure and pixel-level detail. Specifically, UAE features an innovative frequency-band modulator that factorizes real-world content into a fundamental semantic band and residual pixel bands with controllable fine granularity. This design is not only grounded in comprehensive empirical evidence but also validated across diverse reconstruction and perception tasks. With its compact yet semantically expressive representations, UAE outperforms concurrent RAE [50], SVG [34], and UniFlow [48] across rFID, PSNR, gFID and Accuracy metrics on ImageNet, demonstrating that its learned latent space is both semantically representative and pixel-faithful.

Our work makes the following contributions.

1. We introduce the Prism Hypothesis, a unified spectral perspective connecting natural inputs via a shared fundamental band and distinct modality-specific bands, sup-

ported by extensive empirical observations.

2. We present Unified Autoencoding, a simple yet effective tokenizer that combines a frequency band modulator and seamlessly aligns with existing diffusion transformers.
3. Our UAE demonstrates optimal reconstruction quality on ImageNet and MS-COCO together with diffusion-friendly latents, and extensive ablations prove the effectiveness of the proposed frequency-band factorization.

2. Related Work

Unified Tokenizers and Unified Representations. Unifying the representations between pixel and semantic embeddings has become a central objective for existing foundation models. Joint embedding approaches align images and text in a shared representation and enable strong zero-shot transfer [15, 29], and have been extended to many modalities, *e.g.*, audio, depth, thermal, and inertial signals [8]. In parallel, modality-agnostic backbones aim to build a unified architecture that can process diverse input modalities and generate task-specific outputs through learned queries or a shared token representation [1, 14, 23, 24, 42].

On the tokenizer side, discrete codebook methods have demonstrated that the design and granularity of visual tokens play a crucial role in determining how effectively a single sequence model can adapt to vision tasks [6, 47]. Recent work goes further and seeks tokenizers that support both understanding and generation at the same time. OmniTokenizer [41] learns a joint image video tokenizer with a spatial-temporal decoupled transformer and reports strong reconstruction and synthesis across both domains. Very recent studies deepen this trend. UniFlow [48] proposes a unified pixel flow tokenizer that adapts a pretrained encoder through layer-wise self-distillation and employs a lightweight patch-wise flow decoder, explicitly targeting the long-standing tension between semantic abstraction and pixel-faithful reconstruction. Two concurrent works remove the traditional variational bottleneck entirely and build unified representation latents for diffusion transformers. Diffusion Transformers with Representation Autoencoders (RAE) [50] replace the usual reconstruction-only encoder with a pretrained representation encoder, *e.g.*, DINO or SigLIP, and a trained decoder, arguing that semantically rich latents accelerate convergence and improve generative fidelity. SVG [34] trains a diffusion model on DINO features with a small residual branch for details, reporting faster training, few-step sampling, and improved quality.

Our UAE aligns with this shift. It serves as a unified tokenizer that decouples continuous latent features explicitly corresponding to the underlying spectral structure by factorizing real-world contents into a low-frequency base and residual high-frequency bands. It anchors semantics in the core representation while relegating fine-grained details to residuals for progressive reconstruction.

Frequency and Multi-Resolution Modeling. Classical image synthesis adopted pyramids and wavelets to separate structure by scale, enabling coarse-to-fine generation and targeted refinement of detail. A typical example is the Laplacian pyramid of adversarial networks [5], which trains a generator per level and synthesizes images by successively adding higher-frequency residuals. Subsequent analyses of neural networks from a spectral perspective showed that standard architectures prioritize low frequencies and learn higher frequencies later, a phenomenon known as spectral bias [30]. Two lines of work respond to this bias. The first uses input or architecture design to improve access to high frequencies, *e.g.*, Fourier feature mappings and periodic activations that help multi-layer perceptrons represent fine detail [35, 38]. The second introduces frequency-aware objectives and signal processing choices, such as focal frequency loss to emphasize hard frequencies and alias-free synthesis to avoid spurious high-frequency artifacts [16, 17].

Modern generative models retain this multi-resolution view. Cascaded diffusion trains models at increasing resolutions, allowing each stage to learn the appropriate frequency band and its own error distribution [10]. Variants construct explicit feature pyramids or hierarchical patch schedules, enabling efficient diffusion on large images and video while preserving high-frequency detail [7, 36]. Recent latent diffusion designs introduce cross-magnification spaces or zoomable pyramids that share information across scales and enable large-image reconstruction without retraining [45]. In autoregressive models, VAR [40] casts generation as predicting the next scale or resolution, showing strong ImageNet results and clean scaling trends. This explicit progression from global layout to fine detail emerges as a viable alternative to diffusion. Building on this idea, Next Visual Granularity (NVG) generation [?] produces sequences at a fixed resolution but with progressively finer token granularity, surpassing prior VAR baselines while maintaining structured control over detail. Similarly, NFIG [13] performs discrete next-frequency prediction, demonstrating strong generative performance on the ImageNet benchmark. Our approach aligns with these trends but focuses on unified representation rather than the generator’s training schedule.

3. Methodology

3.1. Preliminary Findings

The Prism Hypothesis. Natural inputs are regarded as projections of a common real-world signal onto a shared frequency spectrum. Semantic encoders emphasize a compact low-band that carries categories, attributes, and relations, while pixel encoders observe the same fundamental base together with higher bands that encode edges, textures, and fine appearance. The hypothesis indicates that cross-modal alignment depends primarily on the shared low band.

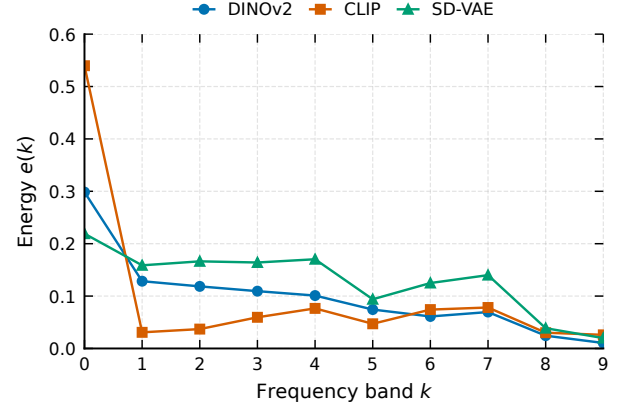


Figure 2. **Frequency energy distribution.** Normalized energy $e(k)$ across frequency bands for diverse tokenizers. DINOv2 and CLIP focus on low-frequency (semantic) content, while SD-VAE retains more high-frequency energy, capturing finer details.

Formalization. Here, \mathcal{F} and \mathcal{F}^\dagger denote two-dimensional discrete Fourier transform and its inverse. For an image $I \in [0, 1]^{3 \times H \times W}$ and a smooth radial mask $\mathbf{M}_\rho^{\text{LP}}$ that passes frequencies within normalized radius $\rho \in (0, 1]$,

$$I_\rho^{\text{LP}} = \mathcal{F}^\dagger(\mathbf{M}_\rho^{\text{LP}} \odot \mathcal{F}(I)), \quad (1)$$

$$I_\rho^{\text{HP}} = \mathcal{F}^\dagger(\mathbf{M}_\rho^{\text{HP}} \odot \mathcal{F}(I)), \quad (2)$$

where $\mathbf{M}_\rho^{\text{HP}}$ is complementary to $\mathbf{M}_\rho^{\text{LP}}$, and both masks use cosine transitions to limit ringing artifacts. All filtering is performed in linear space prior to any model-specific normalization. With a frozen vision-language encoder E , we compute cosine similarities between text embeddings and image embeddings from I , I_ρ^{LP} , and I_ρ^{HP} . If semantic alignment is carried by the shared base, then the retrieval score \mathcal{R} satisfies $\mathcal{R}_{\text{LP}}(\rho)$ is nondecreasing in ρ , $\mathcal{R}_{\text{HP}}(\rho)$ is nonincreasing in ρ , and $\mathcal{R}_{\text{HP}}(\rho)$ approaches chance once the shared base is removed.

Empirical Verification. Here, we validate the *Prism Hypothesis* via two complementary analyses: frequency energy decomposition and retrieval robustness under spectral filtering. **Exp1:** In Figure 2, we first measure the normalized frequency energy distribution $e(k)$ across encoders by averaging the magnitude spectrum of each latent feature channel. This metric quantifies how much representational energy is allocated to each frequency band, revealing that semantic encoders such as DINOv2 and CLIP concentrate most of their energy in the low-frequency region ($k=0$), whereas pixel-oriented models like SD-VAE retain stronger mid- and high-frequency components that capture fine details. **Exp2:** To assess how these spectral tendencies affect semantic alignment, we conduct a controlled retrieval experiment in Figure 4, using text-image retrieval recall (R@5) as the evaluation metric. Images are progressively filtered with radial low-pass or high-pass masks of

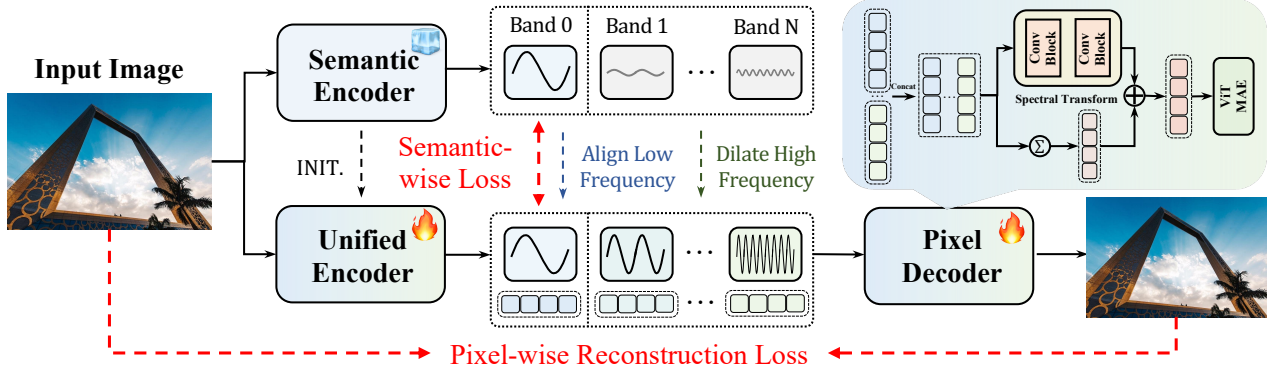


Figure 3. **Overall architecture of our proposed Unified Autoencoding (UAE).** The input image is separately encoded by both a pre-trained *Semantic Encoder* (e.g., DINOv2) and the trainable *Unified Encoder*. The unified encoder is initialized from the semantic encoder and optimized under two complementary objectives: a **semantic-wise loss** that aligns low-frequency components decomposed from the semantic encoder’s representations, and a **pixel-wise reconstruction loss** that enforces visual fidelity via the *Pixel Decoder* by adaptively dilating the high-frequency components. The decoder employs spectral transform blocks to refine residual-frequency content and produce the reconstructed image. This joint optimization harmonizes semantic structure and pixel detail within a single latent space.

increasing cutoff (fraction of Nyquist), while text features remain unchanged. R@5 remains stable under low-pass filtering until the lowest bands are removed, but drops sharply under high-pass filtering, approaching random chance. Together, these results confirm that cross-modal alignment and semantic consistency primarily reside in the shared low-frequency base of the latent spectrum, while higher bands encode modality-specific, fine-grained visual detail.

3.2. Unified AutoEncoder

Using DINOv2 as an example, we initialize our UAE from the pretrained model and remove the register tokens, leaving C channel patch tokens. Input images are center-cropped and resized to the encoder input size, *i.e.*, 224. The resulting tokens are then reshaped into a latent grid $\mathbf{z} \in \mathbb{R}^{B \times C \times H \times W}$ for subsequent frequency-domain processing.

3.3. Residual Split Flow

Given a latent grid $\mathbf{z} \in \mathbb{R}^{B \times C \times H \times W}$, we decompose \mathbf{z} into K frequency bands $\mathbf{z}_f \in \mathbb{R}^{B \times K \times C \times H \times W}$ using an *FFT Band Projector* followed by an *Iterative Split* procedure. Inspired by the coupling mechanism in flow-based models such as Glow [18], the decomposition is performed in the frequency domain via FFT-based projection, allowing each band to capture a distinct spectral component while maintaining invertibility and spatial consistency.

FFT Band Projector. To isolate frequency components, we first apply a two-dimensional discrete Fourier transform to the latent grid, obtaining complex-valued spectral coefficients. Each frequency band is defined by a smooth radial mask M_k , which partitions the Fourier magnitude into K concentric rings. These masks overlap slightly to ensure

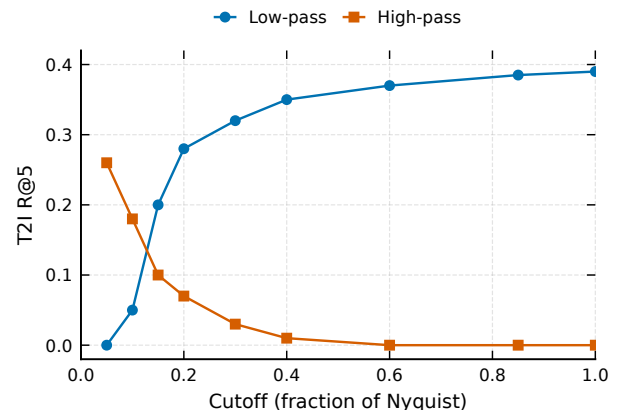


Figure 4. **Retrieval results via frequency filtering.** Text–Image retrieval (R@5) remains stable under low-pass filtering but degrades sharply under high-pass filtering, confirming that semantic alignment primarily resides in low-frequency components.

continuity across spectral boundaries and to prevent ringing artifacts when reconstructed. For each band k , they are transformed back to the spatial domain via an inverse FFT, yielding a spatially coherent band-limited feature.

Iterative Split. With the latent representation $\mathbf{z}_f^{(0)} = \mathbf{z}$, and residual of frequency $\mathbf{r}^{(0)} = \mathbf{z}$, we iteratively decompose the original feature into K frequency bands as:

$$\mathbf{z}_f^{(k)} = \mathcal{P}_k(\mathbf{r}^{(k)}), \quad (3)$$

where the residual term \mathbf{r} is defined as:

$$\mathbf{r}^{(k+1)} = \mathbf{r}^{(k)} - \mathcal{P}_k(\mathbf{r}^{(k)}). \quad (4)$$

Here, \mathcal{P}_k denotes the *FFTBandProjector* corresponding to the k -th radial mask M_k . At the first step ($k=0$), the low-

frequency base $\mathbf{b}^{(0)}$ is directly extracted without residual subtraction. For subsequent steps ($k > 0$), the per-band latent $\mathbf{z}_f^{(k)}$ is progressively calculated by removing each extracted band. After K iterations, the decomposition yields the full set $\{\mathbf{z}_f^{(k)}\}_{k=0}^{K-1}$ as multi-band latent representations.

This residual decomposition encourages spectral disentanglement in one latent space. Low-frequency bands encode global semantics and smooth structures, while higher-frequency bands capture localized edges and fine details.

3.4. Frequency Band Modulator

After the latent representation \mathbf{z} is decomposed into multiple frequency bands, the bands are processed by the frequency modulation module, mapped back to the spatial domain, and then passed through the ViT decoder to reconstruct the RGB image. During training, the multi-band latent is first processed by a noise injection module that perturbs only the high-frequency bands to improve robustness. The resulting latent is then passed through a spectral transform module, which maps it back to the spatial domain before being decoded by the ViT-based pixel decoder.

Noise Injection. To further boost the capacity of the decoder, we perform noise corruption during the training. Specifically, we build a binary condition $\mathbf{m} \in \{0, 1\}^{B \times K}$ indicating which bands are kept from corruption. For each band tensor $\mathbf{b}^{(k)}$ we form noise injection through:

$$\tilde{\mathbf{b}}^{(k)} = \mathbf{m}_{:,k} \odot \mathbf{b}^{(k)} + \bar{\mathbf{m}}_{:,k} \odot \mathcal{N}(\mathbf{0}, \sigma^2 \mathbf{I}), \quad (5)$$

where σ is drawn from $[0, 1]$.

Spectral Transform. As shown in Figure 3, we concatenate processed bands along channels, obtain $\mathbf{s} = \text{Concat}_{\text{ch}}\left(\{\hat{\mathbf{b}}^{(k)}\}_{k=0}^{K-1}\right) \in \mathbb{R}^{B \times KC \times H \times W}$, and pass \mathbf{s} through a two layer convolutional block with SiLU to predict a residual $\Delta \in \mathbb{R}^{B \times C \times H \times W}$. Note that the final fused latent can be formulated as follows:

$$\mathbf{q} = \Delta + \sum_{k=0}^{K-1} \hat{\mathbf{b}}^{(k)} \in \mathbb{R}^{B \times C \times H \times W}. \quad (6)$$

Notably, this tensor \mathbf{q} maintains the same shape as the encoder output, regardless of how many bands are retained, and is the only tensor consumed by the decoder.

3.5. Semantic-wise Loss

To retain the semantic priors of the pretrained teacher while expanding frequency coverage, we apply a *semantic-wise loss* between the unified encoder and the frozen semantic encoder on the lowest K_{base} frequency bands only. Let \mathbf{f}_s and \mathbf{f}_u denote the features from the pretrained-semantic encoders and trainable-unified encoders, respectively. After

frequency decomposition, we obtain band-wise representations $\{\mathbf{f}_s^k\}_{k=0}^{K-1}$ and $\{\mathbf{f}_u^k\}_{k=0}^{K-1}$. The semantic alignment is enforced only for the first K_{base} (low-frequency) bands that encode global structure and object semantics:

$$\mathcal{L}_{\text{sem}} = \frac{\sum_{k=0}^{K_{\text{base}}-1} \|\mathbf{f}_u^k - \mathbf{f}_s^k\|_2^2}{K_{\text{base}}}. \quad (7)$$

This restricted alignment ensures that UAE inherits the semantic layout and category-level organization from the teacher in the low-frequency domain, while leaving the remaining high-frequency bands unconstrained for learning modality-specific, pixel-level detail. In practice, this selective supervision stabilizes training and encourages the unified encoder to harmonize semantic and pixel representations without collapsing into purely pixel features. Noted that in our experiments, we set $K_{\text{base}} = 1$ by default.

4. Experiments

4.1. Implementation Details

Dataset. Following the standard settings, we train our UAE on ImageNet-1K train set and evaluate it on ImageNet-1K val set and MS-COCO 2017 dataset for fair comparisons.

Training Settings. We train UAE with DINoV2-B and DINoV2-L respectively in 256x256 resolution. The training processes are decomposed into three stages. In stage 1, the semantic encoder is frozen, where the decoder is trained by reconstruction loss. In stage 2, we unfreeze the encoder and finetune the full model with semantic-wise loss and reconstruction loss. In stage 3, we finetune the full model end-to-end with noise injection and GAN loss, where the GAN loss setting follows the representative RAE [50].

4.2. Visual Reconstruction

Quantitative Evaluation. In Table 1, We quantify reconstruction quality at 256×256 on ImageNet-1K and MS-COCO 2017. The compared baselines include widely-used generative tokenizers and variational decoders. For a fair comparison, we report the evaluation results for our UAE and the corresponding baseline that follows the same configurations of DINoV2-base. Here, we report PSNR and SSIM for fidelity, and rFID for perceptual quality.

Notably, our UAE delivers state-of-the-art reconstruction quality among unified tokenizers. On ImageNet-1K, UAE improves over the RAE baseline from 18.05 to 29.65 in PSNR and from 0.50 to 0.88 in SSIM, while reducing FID from 2.04 to 0.19. On MS-COCO, UAE raises PSNR from 18.37 to 29.23 and SSIM from 0.49 to 0.89, with FID decreasing from 2.56 to 0.18. These notable gains validate that moving masking out of the decoder and factorizing latents into a low-frequency base and residual bands preserve fine detail while maintaining semantic structure.

Table 1. **Reconstruction quality on ImageNet-1K and MS-COCO 2017 full set (256x256).** Note that our proposed UAE achieves state-of-the-art reconstruction among unified tokenizers and remains competitive with strong autoencoders such as Flux-VAE and SD3-VAE. Under identical DINOv2 encoders, UAE significantly outperforms the RAE baseline in both PSNR and SSIM while reducing rFID by over 90%. When scaled to DINOv2-L, UAE attains the best overall perceptual quality (rFID=0.16) and fidelity (PSNR=33.08, SSIM=0.94), demonstrating the effectiveness of frequency-aware factorization in preserving both semantic and fine-grained visual detail.

Method	Type	Ratio	ImageNet-1K			MS-COCO 2017		
			PSNR↑	SSIM↑	rFID↓	PSNR↑	SSIM↑	rFID↓
SD-VAE [32]	Continuous	8	25.68	0.72	0.75	25.43	0.73	0.76
SD-VAE-EMA [32]	Continuous	8	24.99	0.71	0.63	24.76	0.72	0.57
SD3-VAE [22]	Continuous	8	29.58	0.86	0.21	29.50	0.87	0.19
Flux-VAE [20]	Continuous	8	31.07	0.89	0.17	30.99	0.90	0.19
TokenFlow [28]	Discrete	16	21.41	0.69	1.37	-	-	-
DualViTok [11]	Discrete	16	22.53	0.74	1.37	-	-	-
EMU2 [37]	Continuous	14	13.49	0.42	3.27	-	-	-
UniLIP [39]	Continuous	32	22.99	0.75	0.79	-	-	-
RAE (DINOv2-B)	Continuous	14	18.05	0.5	2.04	18.37	0.49	2.56
UAE (DINOv2-B)	Continuous	14	29.65	0.88	0.19	29.23	0.89	0.18
UniFlow (DINOv2-L)	Continuous	14	32.32	0.91	0.17	32.29	0.90	0.18
UAE (DINOv2-L)	Continuous	14	33.08	0.94	0.16	32.84	0.94	0.17



Figure 5. **Qualitative comparison of reconstruction fidelity across autoencoding paradigms.** We visualize reconstructed samples from representative methods, including SD-VAE [33], RAE [50], and our proposed UAE. Each row corresponds to reconstructions from a fixed source set spanning text, human, object, and artistic domains. UAE produces the most consistent and semantically faithful reconstructions, preserving both high-frequency details (e.g., texture and edge sharpness) and global structure (e.g., layout and color harmony), while reducing the blurring and semantic drift observed in SD-VAE and RAE. (The detail comparisons are denoted in the yellow boxes.)

Beyond unified tokenizers, UAE is competitive with the best generative-only tokenizers. On ImageNet-1K, UAE at-

tains an FID of 0.19, matching SD three VAE and approaching Flux VAE, while maintaining high PSNR and SSIM. A

Table 2. **Class-conditional generation performance on ImageNet (256x256).** We compare our proposed UAE with recent diffusion and autoregressive models using standard metrics. Note that the UAE performs generation in a causal manner, progressing from low- to high-frequency bands in the latent space.

	gFID \downarrow	IS \uparrow	Prec \uparrow	Rec \uparrow
DiT-XL/2 [27]	2.27	271.3	0.83	0.57
VAR [40]	1.73	350.2	<u>0.82</u>	0.6
UniFlow [48]	2.45	228.0	-	-
RAE [50]	1.51	242.9	0.79	0.63
UAE	<u>1.68</u>	<u>301.6</u>	0.77	<u>0.61</u>

similar pattern holds on MS-COCO, where UAE equals or surpasses the strongest baselines in perceptual quality.

Qualitative Evaluation. Figure 5 compares source images with the resulting reconstructions from SD-VAE, RAE, and UAE. Note that our UAE can well preserve straight edges, fine textures, and small text, *e.g.*, street signs and printed documents. The improvement is consistent across natural photos and illustrations, as shown by the montage on page one of the uploaded figure. The detailed comparisons are shown in the **yellow** boxes in the images.

4.3. Generative Modeling

To further assess the effectiveness of the proposed UAE, we conduct class-conditional image generation experiments on ImageNet-1K at a resolution of 256×256 .

We conduct all generative experiments in the multi-band latent space. All experimental settings follow those used in RAE [50] to ensure a fair comparison. As shown in Table 2, our UAE attains a gFID of **1.68** and an IS of **301.6**, achieving performance on par with existing state-of-the-art generative models. This suggests that the unified frequency-based representation enables the generative model to progressively capture both global structure and fine-grained details in a coherent manner, keeping highly generative while preserving strong semantic quality. Overall, the UAE latent space, constructed through explicit low- and high-frequency decomposition, provides an effective and diffusion-friendly foundation for large-scale visual generation.

4.4. Semantic Understanding

To evaluate the learned semantic discriminability, we perform linear probing on ImageNet-1K following the standard protocol in [48]. All encoder weights are frozen, and a single linear classifier is trained on top of the global embeddings for 30 epochs using SGD with a cosine learning rate schedule and a base rate of 0.1. Consistent augmentations are applied across methods for a fair comparison.

As shown in Table 3, our UAE achieves a top-1 accuracy of **83.0%** based on a ViT-B backbone, outperforming previ-

Table 3. **Linear probing on ImageNet-1K.** UAE achieves 83.0% top-1 accuracy with a ViT-B backbone, matching RAE and surpassing larger ViT-L models such as MAE, MAGE, and UniFlow. This shows that UAE’s unified latent space preserves strong semantic discriminability with compact model size.

Methods	Size	ACC \uparrow
VFMTok [49]	ViT-L	69.4
BEiT [2]	ViT-L	73.5
MAE [9]	ViT-L	75.8
MAGE [21]	ViT-L	78.9
UniFlow [48]	ViT-L	82.6
RAE [50]	ViT-B	83.0
UAE	ViT-B	83.0

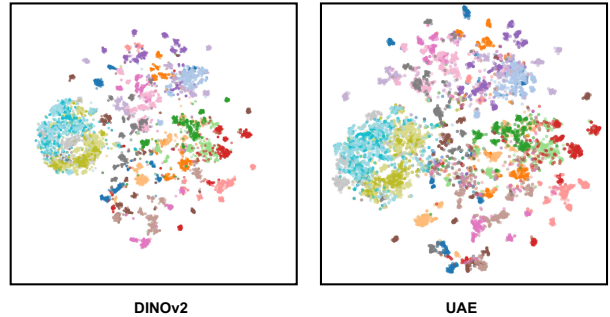


Figure 6. **t-SNE visualization of semantic embeddings.** We compare the feature distributions from the DINOv2 encoder (left) and the band-0 (low-frequency) component of UAE (right). The two plots exhibit similar global structures and class separability, indicating that UAE effectively preserves the semantic organization of the original encoder while introducing a unified latent space that remains compatible with frequency-based factorization.

ous self-supervised and tokenizer-based approaches. Compared to VFMTok (69.4%) and BEiT (73.5%), our UAE exhibits a substantial improvement, demonstrating that the unified latent space preserves stronger semantic alignment. Even against large-scale models such as MAGE (78.9%) and UniFlow (82.6%), UAE maintains competitive classification accuracy despite its smaller backbone.

To further visualize this property, Figure 6 shows t-SNE comparisons between the DINOv2 encoder and the band-0 (low-frequency) component of UAE. The two plots share highly similar global structures and class separability, confirming that UAE’s low-frequency representations retain the original semantic organization of DINOv2, while enabling a unified latent space compatible with frequency-based factorization. This qualitative visualization supports our design goal of preserving global semantics while enriching fine-grained visual detail in higher-frequency bands.

Table 4. **Configurations of UAE modules.** Progressively integrating various strategies improves both fidelity and perceptual realism. The BandProjector enhances structure recovery, tuning pre-trained encoders largely improves pixel-level fidelity, and noise injection stabilizes training for the best reconstruction quality.

Methods	PSNR \uparrow	SSIM \uparrow	rFID \downarrow
Baseline	15.27	0.45	22.98
+ BandProjector	22.13	0.71	15.22
+ Tuning Encoder	29.02	0.88	0.21
+ Noise Injection	29.65	0.88	0.19

Table 5. **Configurations different band splits.** UAE maintains consistent and stable reconstruction and semantic performance across different numbers of frequency bands, demonstrating the robustness of the proposed frequency factorization design.

Bands	PSNR \uparrow	SSIM \uparrow	rFID \downarrow	ACC \uparrow
10	29.65	0.88	0.19	83.0
8	29.37	0.88	0.19	83.0
6	29.41	0.88	0.19	83.0
4	29.52	0.88	0.19	83.0
2	29.55	0.88	0.19	83.0

5. Ablation Study

5.1. The Effectiveness of the UAE Modules

In Table 4, we evaluate the influence of each core configuration in our proposed UAE on ImageNet-1K. Starting from a baseline that directly reconstructs images from the frozen DINOv2-B encoder, we progressively add the *BandProjector*, *Encoder Tuning*, and *Noise Injection* strategies.

Note that these components introduce solid and progressive improvements for visual fidelity. The BandProjector enhances structural recovery by decomposing latent signals across frequency bands, increasing PSNR from 15.27 to 22.13 and SSIM from 0.45 to 0.71. Tuning the encoder further aligns the latent representation with the reconstruction objective, raising PSNR to 27.02 and reducing rFID from 15.22 to 7.81. Finally, the noise injection strategy yields a large gain, achieving PSNR 29.65, SSIM 0.88, and rFID 0.19, indicating impressive perceptual fidelity.

Together, these results confirm that frequency decomposition, semantic alignment, and controlled noise regularization jointly enable UAE to harmonize semantic structure and fine visual detail in one unified representation space.

5.2. The Configurations of Band Splits

We further examine how the number of frequency bands affects reconstruction fidelity and semantic consistency. In Table 5, varying the number of bands from 2 to 10 produces nearly identical performance across all metrics: PSNR stays

Table 6. **Semantic comparisons in DINOv2.** Comparison of classification accuracy when probing different representations derived from DINOv2. **Band₀** denotes using only the lowest-frequency band for linear probing, whereas **Concat** refers to probing with the concatenation of all frequency-band representations.

Methods	DINOv2	Band ₀	Concat
Accuracy(%)	83.0	83.3	83.0

around 29, SSIM remains at 0.88, rFID is consistently 0.19, and linear probing accuracy (ACC) stays fixed at 83.0%.

These results demonstrate that UAE’s frequency factorization is highly robust to band granularity. Its decomposition reliably preserves both low-frequency and high-frequency information even when the spectrum is split coarsely. The minimal variation further indicates that most of the frequency energy is captured by the base and the first few residual bands, confirming that the unified representation does not depend on fine-grained spectral partitioning.

In practice, using fewer bands slightly reduces computation without harming reconstruction quality or downstream performance. With more multi-frequency latents, our UAE also naturally supports iterative image generation.

5.3. The Semantic Comparisons in DINOv2

As shown in Table 6, using only the lowest-frequency component (**Band₀**) achieves slightly higher accuracy (83.3%) than both the original DINOv2 features and the concatenated multi-band representation (83.0%). This indicates that the low-frequency band effectively retains the global semantic structure of DINOv2, which dominates discriminative performance in classification.

6. Conclusion

We propose the Prism Hypothesis, which views diverse natural inputs as projections of a shared spectrum composed of a compact low-frequency semantic component and residual higher-frequency detail. Preliminary experiments about frequency-band distributions of various visual and textual encoders strongly enlighten this connection between feature spectra and representational function. Hence, we launch Unified AutoEncoding (UAE), which harmonizes semantic and pixel information within a single latent space via a hierarchical frequency-band modulator. Extensive experiments confirm that it delivers greater generative capability over existing unified tokenizers, *e.g.*, RAE, SVG, and UniFlow, meanwhile preserving reconstruction quality on par with top-tier models like Flux-VAE. We position the UAE as a promising and practical route towards unified tokenizers for understanding and generation.

References

- [1] Alexei Baevski, Wei-Ning Hsu, Qiantong Xu, Arun Babu, Jiatao Gu, and Michael Auli. Data2vec: A general framework for self-supervised learning in speech, vision and language. In *International conference on machine learning*, pages 1298–1312. PMLR, 2022. 2
- [2] Hangbo Bao, Li Dong, Songhao Piao, and Furu Wei. BEiT: BERT pre-training of image transformers. In *International Conference on Learning Representations*, 2022. 7
- [3] Mathilde Caron, Hugo Touvron, Ishan Misra, Hervé Jégou, Julien Mairal, Piotr Bojanowski, and Armand Joulin. Emerging properties in self-supervised vision transformers. In *Proceedings of the IEEE/CVF international conference on computer vision*, pages 9650–9660, 2021. 1
- [4] Jun Chen, Deyao Zhu, Guocheng Qian, Bernard Ghanem, Zhicheng Yan, Chenchen Zhu, Fanyi Xiao, Sean Chang Culatana, and Mohamed Elhoseiny. Exploring open-vocabulary semantic segmentation from clip vision encoder distillation only. In *Proceedings of the IEEE/CVF International Conference on Computer Vision*, pages 699–710, 2023. 2
- [5] Emily L Denton, Soumith Chintala, Rob Fergus, et al. Deep generative image models using a laplacian pyramid of adversarial networks. *Advances in neural information processing systems*, 28, 2015. 3
- [6] Patrick Esser, Robin Rombach, and Bjorn Ommer. Taming transformers for high-resolution image synthesis. In *Proceedings of the IEEE/CVF conference on computer vision and pattern recognition*, pages 12873–12883, 2021. 2
- [7] Wan-Cyuan Fan, Yen-Chun Chen, DongDong Chen, Yu Cheng, Lu Yuan, and Yu-Chiang Frank Wang. Frido: Feature pyramid diffusion for complex scene image synthesis. In *Proceedings of the AAAI conference on artificial intelligence*, pages 579–587, 2023. 3
- [8] Rohit Girdhar, Alaaeldin El-Nouby, Zhuang Liu, Mannat Singh, Kalyan Vasudev Alwala, Armand Joulin, and Ishan Misra. Imagebind: One embedding space to bind them all. In *Proceedings of the IEEE/CVF conference on computer vision and pattern recognition*, pages 15180–15190, 2023. 2
- [9] Kaiming He, Xinlei Chen, Saining Xie, Yanghao Li, Piotr Dollár, and Ross Girshick. Masked autoencoders are scalable vision learners. In *Proceedings of the IEEE/CVF conference on computer vision and pattern recognition*, pages 16000–16009, 2022. 7
- [10] Jonathan Ho, Chitwan Saharia, William Chan, David J Fleet, Mohammad Norouzi, and Tim Salimans. Cascaded diffusion models for high fidelity image generation. *Journal of Machine Learning Research*, 23(47):1–33, 2022. 3
- [11] Runhui Huang, Chunwei Wang, Junwei Yang, Guansong Lu, Yunlong Yuan, Jianhua Han, Lu Hou, Wei Zhang, Lanqing Hong, Hengshuang Zhao, et al. Illume+: Illuminating unified mllm with dual visual tokenization and diffusion refinement. *arXiv preprint arXiv:2504.01934*, 2025. 1, 6
- [12] Wei Huang, Zhiliang Peng, Li Dong, Furu Wei, Jianbin Jiao, and Qixiang Ye. Generic-to-specific distillation of masked autoencoders. In *Proceedings of the IEEE/CVF conference on computer vision and pattern recognition*, pages 15996–16005, 2023. 2
- [13] Zhihao Huang, Xi Qiu, Yukuo Ma, Yifu Zhou, Junjie Chen, Hongyuan Zhang, Chi Zhang, and Xuelong Li. Nfig: Multi-scale autoregressive image generation via frequency ordering. In *The Thirty-ninth Annual Conference on Neural Information Processing Systems*, 2025. 3
- [14] Andrew Jaegle, Sebastian Borgeaud, Jean-Baptiste Alayrac, Carl Doersch, Catalin Ionescu, David Ding, Skanda Koppara, Daniel Zoran, Andrew Brock, Evan Shelhamer, et al. Perceiver io: A general architecture for structured inputs & outputs. *arXiv preprint arXiv:2107.14795*, 2021. 2
- [15] Chao Jia, Yinfai Yang, Ye Xia, Yi-Ting Chen, Zarana Parekh, Hieu Pham, Quoc Le, Yun-Hsuan Sung, Zhen Li, and Tom Duerig. Scaling up visual and vision-language representation learning with noisy text supervision. In *International conference on machine learning*, pages 4904–4916. PMLR, 2021. 2
- [16] Liming Jiang, Bo Dai, Wayne Wu, and Chen Change Loy. Focal frequency loss for image reconstruction and synthesis. In *Proceedings of the IEEE/CVF international conference on computer vision*, pages 13919–13929, 2021. 3
- [17] Tero Karras, Miika Aittala, Samuli Laine, Erik Härkönen, Janne Hellsten, Jaakko Lehtinen, and Timo Aila. Alias-free generative adversarial networks. *Advances in neural information processing systems*, 34:852–863, 2021. 3
- [18] Durk P Kingma and Prafulla Dhariwal. Glow: Generative flow with invertible 1x1 convolutions. *Advances in neural information processing systems*, 31, 2018. 4
- [19] Diederik P Kingma and Max Welling. Auto-encoding variational bayes. *arXiv preprint arXiv:1312.6114*, 2013. 1
- [20] Black Forest Labs, Stephen Batifol, Andreas Blattmann, Frederic Boesel, Saksham Consul, Cyril Diagne, Tim Dockhorn, Jack English, Zion English, Patrick Esser, et al. Flux. 1 kontext: Flow matching for in-context image generation and editing in latent space. *arXiv preprint arXiv:2506.15742*, 2025. 6
- [21] Tianhong Li, Huiwen Chang, Shlok Mishra, Han Zhang, Dina Katabi, and Dilip Krishnan. Mage: Masked generative encoder to unify representation learning and image synthesis. In *Proceedings of the IEEE/CVF Conference on Computer Vision and Pattern Recognition*, pages 2142–2152, 2023. 7
- [22] Joshua Lopez. Stable diffusion 3: Research paper. <https://stability.ai/news/stable-diffusion-3-research-paper>, 2025. Stability AI. 6
- [23] Jiasen Lu, Christopher Clark, Rowan Zellers, Roozbeh Mottaghi, and Aniruddha Kembhavi. Unified-io: A unified model for vision, language, and multi-modal tasks. *arXiv preprint arXiv:2206.08916*, 2022. 2
- [24] Jiasen Lu, Christopher Clark, Sangho Lee, Zichen Zhang, Savya Khosla, Ryan Marten, Derek Hoiem, and Aniruddha Kembhavi. Unified-io 2: Scaling autoregressive multimodal models with vision language audio and action. In *Proceedings of the IEEE/CVF Conference on Computer Vision and Pattern Recognition*, pages 26439–26455, 2024. 2
- [25] Duy-Kien Nguyen, Mahmoud Assran, Unnat Jain, Martin R Oswald, Cees GM Snoek, and Xinlei Chen. An image is worth more than 16x16 patches: Exploring transformers on individual pixels. *arXiv preprint arXiv:2406.09415*, 2024. 1

- [26] Maxime Oquab, Timothée Darcet, Théo Moutakanni, Huy Vo, Marc Szafraniec, Vasil Khalidov, Pierre Fernandez, Daniel Haziza, Francisco Massa, Alaaeldin El-Nouby, et al. Dinov2: Learning robust visual features without supervision. *arXiv preprint arXiv:2304.07193*, 2023. 1
- [27] William Peebles and Saining Xie. Scalable diffusion models with transformers. In *Proceedings of the IEEE/CVF international conference on computer vision*, pages 4195–4205, 2023. 7
- [28] Liao Qu, Huichao Zhang, Yiheng Liu, Xu Wang, Yi Jiang, Yiming Gao, Hu Ye, Daniel K Du, Zehuan Yuan, and Xinglong Wu. Tokenflow: Unified image tokenizer for multimodal understanding and generation. In *Proceedings of the Computer Vision and Pattern Recognition Conference*, pages 2545–2555, 2025. 1, 6
- [29] Alec Radford, Jong Wook Kim, Chris Hallacy, Aditya Ramesh, Gabriel Goh, Sandhini Agarwal, Girish Sastry, Amanda Askell, Pamela Mishkin, Jack Clark, et al. Learning transferable visual models from natural language supervision. In *International conference on machine learning*, pages 8748–8763. PMLR, 2021. 1, 2
- [30] Nasim Rahaman, Aristide Baratin, Devansh Arpit, Felix Draxler, Min Lin, Fred Hamprecht, Yoshua Bengio, and Aaron Courville. On the spectral bias of neural networks. In *International conference on machine learning*, pages 5301–5310. PMLR, 2019. 3
- [31] Ali Razavi, Aaron Van den Oord, and Oriol Vinyals. Generating diverse high-fidelity images with vq-vae-2. *Advances in neural information processing systems*, 32, 2019. 1
- [32] Robin Rombach, Andreas Blattmann, Dominik Lorenz, Patrick Esser, and Björn Ommer. High-resolution image synthesis with latent diffusion models. In *Proceedings of the IEEE/CVF conference on computer vision and pattern recognition*, pages 10684–10695, 2022. 6
- [33] Robin Rombach, Andreas Blattmann, Dominik Lorenz, Patrick Esser, and Björn Ommer. High-resolution image synthesis with latent diffusion models. In *Proceedings of the IEEE/CVF conference on computer vision and pattern recognition*, pages 10684–10695, 2022. 6
- [34] Minglei Shi, Haolin Wang, Wenzhao Zheng, Ziyang Yuan, Xiaoshi Wu, Xintao Wang, Pengfei Wan, Jie Zhou, and Jiwen Lu. Latent diffusion model without variational autoencoder. *arXiv preprint arXiv:2510.15301*, 2025. 2
- [35] Vincent Sitzmann, Julien Martel, Alexander Bergman, David Lindell, and Gordon Wetzstein. Implicit neural representations with periodic activation functions. *Advances in neural information processing systems*, 33:7462–7473, 2020. 3
- [36] Ivan Skorokhodov, Willi Menapace, Aliaksandr Siarohin, and Sergey Tulyakov. Hierarchical patch diffusion models for high-resolution video generation. In *Proceedings of the IEEE/CVF Conference on Computer Vision and Pattern Recognition*, pages 7569–7579, 2024. 3
- [37] Quan Sun, Yufeng Cui, Xiaosong Zhang, Fan Zhang, Qiyi- ing Yu, Yueze Wang, Yongming Rao, Jingjing Liu, Tiejun Huang, and Xinlong Wang. Generative multimodal models are in-context learners. In *Proceedings of the IEEE/CVF Conference on Computer Vision and Pattern Recognition*, pages 14398–14409, 2024. 6
- [38] Matthew Tancik, Pratul Srinivasan, Ben Mildenhall, Sara Fridovich-Keil, Nithin Raghavan, Utkarsh Singhal, Ravi Ramamoorthi, Jonathan Barron, and Ren Ng. Fourier features let networks learn high frequency functions in low dimensional domains. *Advances in neural information processing systems*, 33:7537–7547, 2020. 3
- [39] Hao Tang, Chenwei Xie, Xiaoyi Bao, Tingyu Weng, Pandeng Li, Yun Zheng, and Liwei Wang. Unilip: Adapting clip for unified multimodal understanding, generation and editing. *arXiv preprint arXiv:2507.23278*, 2025. 1, 6
- [40] Keyu Tian, Yi Jiang, Zehuan Yuan, Bingyue Peng, and Liwei Wang. Visual autoregressive modeling: Scalable image generation via next-scale prediction. *Advances in neural information processing systems*, 37:84839–84865, 2024. 3, 7
- [41] Junke Wang, Yi Jiang, Zehuan Yuan, Bingyue Peng, Zuxuan Wu, and Yu-Gang Jiang. Omnitokenizer: A joint image-video tokenizer for visual generation. *Advances in Neural Information Processing Systems*, 37:28281–28295, 2024. 2
- [42] Wenhui Wang, Hangbo Bao, Li Dong, Johan Bjorck, Zhihui Peng, Qiang Liu, Kriti Aggarwal, Owais Khan Mohammed, Saksham Singhal, Subhajit Som, et al. Image as a foreign language: Beit pretraining for vision and vision-language tasks. In *Proceedings of the IEEE/CVF Conference on Computer Vision and Pattern Recognition*, pages 19175–19186, 2023. 2
- [43] Ji-Jia Wu, Andy Chia-Hao Chang, Chieh-Yu Chuang, Chun-Pei Chen, Yu-Lun Liu, Min-Hung Chen, Hou-Ning Hu, Yung-Yu Chuang, and Yen-Yu Lin. Image-text co-decomposition for text-supervised semantic segmentation. In *Proceedings of the IEEE/CVF Conference on Computer Vision and Pattern Recognition*, pages 26794–26803, 2024. 2
- [44] Jiarui Xu, Shalini De Mello, Sifei Liu, Wonmin Byeon, Thomas Breuel, Jan Kautz, and Xiaolong Wang. Groupvit: Semantic segmentation emerges from text supervision. In *Proceedings of the IEEE/CVF conference on computer vision and pattern recognition*, pages 18134–18144, 2022. 2
- [45] Srikanth Yellapragada, Alexandros Graikos, Kostas Triaridis, Prateek Prasanna, Rajarsi Gupta, Joel Saltz, and Dimitris Samaras. Zoomldm: Latent diffusion model for multi-scale image generation. In *Proceedings of the Computer Vision and Pattern Recognition Conference*, pages 23453–23463, 2025. 3
- [46] Muyang Yi, Quan Cui, Hao Wu, Cheng Yang, Osamu Yoshie, and Hongtao Lu. A simple framework for text-supervised semantic segmentation. In *Proceedings of the IEEE/CVF Conference on Computer Vision and Pattern Recognition*, pages 7071–7080, 2023. 2
- [47] Lijun Yu, José Lezama, Nitesh B Gundavarapu, Luca Ver- sari, Kihyuk Sohn, David Minnen, Yong Cheng, Vighnesh Birodkar, Agrim Gupta, Xiuye Gu, et al. Language model beats diffusion–tokenizer is key to visual generation. *arXiv preprint arXiv:2310.05737*, 2023. 2
- [48] Zhengrong Yue, Haiyu Zhang, Xiangyu Zeng, Boyu Chen, Chenting Wang, Shaobin Zhuang, Lu Dong, KunPeng Du, Yi Wang, Limin Wang, et al. Uniflow: A unified pixel flow tokenizer for visual understanding and generation. *arXiv preprint arXiv:2510.10575*, 2025. 2, 7

- [49] Anlin Zheng, Xin Wen, Xuanyang Zhang, Chuofan Ma, Tiancai Wang, Gang Yu, Xiangyu Zhang, and Xiaojuan Qi. Vision foundation models as effective visual tokenizers for autoregressive image generation. *arXiv preprint arXiv:2507.08441*, 2025. [7](#)
- [50] Boyang Zheng, Nanye Ma, Shengbang Tong, and Saining Xie. Diffusion transformers with representation autoencoders. *arXiv preprint arXiv:2510.11690*, 2025. [2](#), [5](#), [6](#), [7](#)